Review of Scientific Instruments

A new type of hydrothermal diamond-anvil cell with cooling system

Cite as: Rev. Sci. Instrum. **91**, 053104 (2020); https://doi.org/10.1063/1.5143596
Submitted: 26 December 2019 . Accepted: 24 April 2020 . Published Online: 19 May 2020

Jiankang Li, I-Ming Chou, W. A. Bassett, and Xian Wang

Review of Scientific Instruments ARTICLE scitation.org/journal/rsi

A new type of hydrothermal diamond-anvil cell with cooling system

Cite as: Rev. Sci. Instrum. 91, 053104 (2020); doi: 10.1063/1.5143596
Submitted: 26 December 2019 • Accepted: 24 April 2020 •
Published Online: 19 May 2020

Jiankang Li,[1,a)] I-Ming Chou,[2] W. A. Bassett,[3] and Xian Wang[4]

AFFILIATIONS

[1]MNR Key Laboratory of Metallogeny and Mineral Assessment, Institute of Mineral Resources, Chinese Academy of Geological Sciences, Beijing 100037, China
[2]CAS Key Laboratory of Experimental Study Under Deep-sea Extreme Conditions, Institute of Deep-Sea Science and Engineering, Chinese Academy of Sciences, Sanya, Hainan 572000, China
[3]Department of Earth and Atmospheric Sciences, Cornell University, Ithaca, New York 14853, USA
[4]State Key Laboratory of Geological Processes and Mineral Resources, China University of Geosciences (Beijing), Beijing 100083, China

[a)]**Author to whom correspondence should be addressed:** Li9968@126.com

ABSTRACT

A new type of hydrothermal diamond-anvil cell (HDAC-VII) and its accompanied cooling system were designed. The design of HDAC-VII in which the three posts work simultaneously as guideposts and screw posts greatly shortened the horizontal size of HDAC compared with older types. It provides more open space and shorter distance to analyze and observe the sample chamber from side access. Moreover, four ports were used to connect the upper and lower spaces between windows and anvils, so mixed gas (Ar + H_2) can pass through both of them. In the heating experiments, the mixed gas prevents diamond anvils and other parts from being oxidized as well as cooling the observing windows. Dry gas can be passed through those spaces during cooling, preventing condensation on the table faces of anvils and the observing windows. The cooling system can cool the sample chamber to −170 °C with an accuracy of ±0.5 °C by using a nitrogen stream cooled through a stainless steel coil immersed in a liquid nitrogen Dewar. The heating rates while reheating a frozen sample can be controlled to be 0.1 °C/min with a temperature fluctuation of 0.1 °C. These improvements extend the HDAC applications especially in low temperature conditions. For example, (1) we measured the salinities of NaCl–H_2O loaded in the sample chamber, (2) we observed the ice I and VI-melting process and correspondingly calculated the density of water in the sample chamber, and (3) we performed lepidolite crystallization in an aqueous solution with 10 wt. % NaCl to simulate its natural forming conditions.

I. INTRODUCTION

Since its invention in 1993 to research the fluid and rock properties under crustal pressure and temperature conditions, the hydrothermal diamond-anvil cells (HDACs) have evolved from type I, III, and V to VT in over 25 years (Bassett *et al.*, 1993; Bassett, 2009; and Li *et al.*, 2016) in order to meet the demands of the different experiments. For example, for x-ray studies, the HDAC-V was designed to provide more space for x rays to pass into and out of the sample chamber than was the case in HDAC-I and HDAC-III and prevent serious interference from emissions resulting from the stainless steel parts between which the x rays had to pass (Anderson *et al.*, 2010). HDAC-V also shortened the distance between the sample chamber and the observing window for making measurements through the microscope lens (Li *et al.*, 2013 and Maneta and Anderson, 2018). Inheriting the merits of HDAC-V, HDAC-VT was designed with more stable properties and became easier for loading samples (Li *et al.*, 2016). However, although the HDAC-V and HDAC-VT became small in size, they are still somewhat too big for many sample stages of equipment, including the microscope and x-ray stage.

On the other hand, it is essential to measure the property of fluid loaded in the sample chamber in frozen condition in many experiments using HDAC. For example, brine solution (e.g., NaCl–H_2O) is common in nature, and the true composition of the brine solution loaded within the HDAC sample chamber is

essential for the interpretation of experimental results. Because the fluid composition in the sealed sample chamber could not be equal to that before loading due to the evaporation while sealing the sample chamber, it is necessary to determine the salinity of the loaded solution by measuring the ice melting temperature (Bodnar, 1993 and Bodnar and Vityk, 1994). Previously, no effective and convenient cooling system was designed to cool the sample chamber of HDAC to form ice and determine its melting temperature. Conventionally, a stream of liquid nitrogen was used to cool the sample chamber of HDAC directly, as reported by Bassett *et al.* (1993). When using this method, it is difficult to control the cooling rates precisely and to minimize low temperature fluctuation of the sample. In addition, a large liquid nitrogen container was used during the cooling experiments, and a considerable amount of liquid nitrogen was wasted.

In this study, we designed a new type of HDAC (HDAC-VII) with smaller size than old types and a cooling system with high accuracy such that the composition of the sample solution can be determined by the measured ice melting temperature (Bodnar, 1993; Bodnar and Vityk, 1994; and Mao and Duan, 2008).

II. DESCRIPTION OF HDAC-VII

HDAC-VII inherits the core designs of HDAC-I, -III, -V, and -VT, including the designs of heaters, ceramic heat barriers, ball joint for orienting the lower anvil, and sliding disk for positioning the upper anvil [Fig. 1 and Fig. 1 in Bassett *et al.* (1993)]. HDAC-VII has three guideposts, the same as HDAC-III and HDAC-VT. The three posts in HDAC-VII have screw threads on the upper ends, which allow them to be used as driver screws to apply pressure on the diamond anvils by turning the nuts simultaneously (Figs. 1–3). Such design, which allows the HDAC-VII to retain the merits of the HDAC-VT, provides the better guidance and more balanced pressure loaded on the anvils than those of the HDAC-V with its two driver screws. As a result, the HDAC-VII can protect the diamonds and other parts of HDAC from being broken under high T–P conditions. Additionally, the HDAC-VII inherits from the HDAC-V and HDAC-VT, the location of the guideposts outside of the collar containing the hot gas chamber, thereby minimizing the chance of seizing or deforming due to heating of the posts.

This design in which the three posts can work simultaneously as guideposts and screw posts greatly shortened the horizontal size of HDAC compared with old types (Fig. 3). Its largest horizontal dimension is 48 mm and its height is 34 mm (Figs. 1 and 3). However, the short distances among the three guideposts make the lateral movement to easily occur. To solve this shortcoming, we used sliding bushings to match the guideposts, which provide higher lateral precision than the linear ball bearings used in the HDAC-VT. In order to ensure that the three bushings in the upper platen and posts in the lower platen can be assembled in high precision, the posts were designed to be removable and were installed in the lower platen with screws. Otherwise, if the posts in the lower platen are not perfectly vertical due to low precision, the bushings and posts could seize up. Additionally, we fix the post in the lower platens with high temperature cement that fills in the gaps between post, screw and lower platen, preventing the post from being loosened while turning nuts on the upper platen to seal the sample chamber.

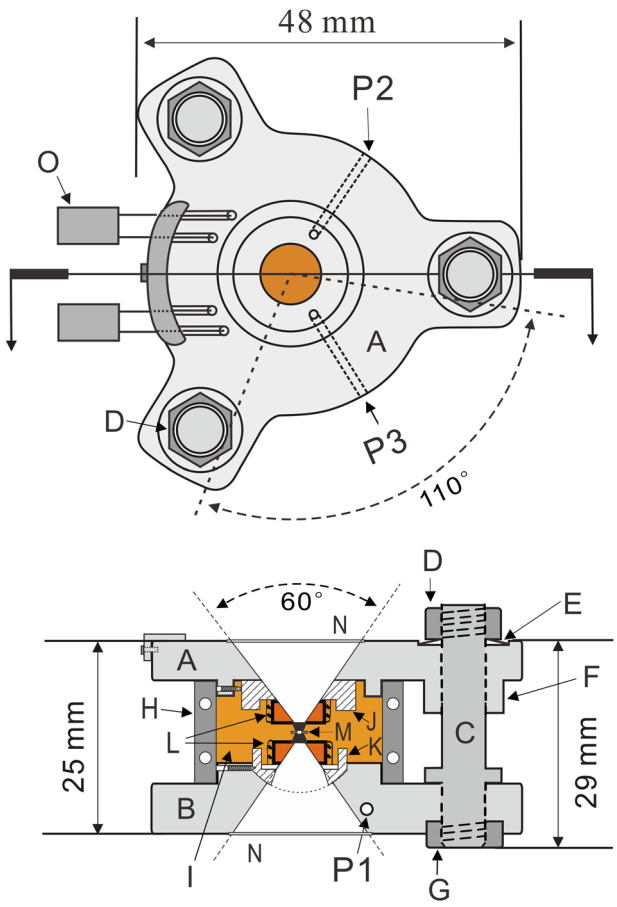

FIG. 1. Schematic diagram showing the design of an HDAC-VII. 60° is the conical opening of both top and bottom windows that allow large solid angles for through-anvil viewing and spectroscopy. 110° is the opening angle on three sides when side access is used. The parts are (A) upper platen, (B) lower platen, (C) three guideposts, (D) upper nut, (E) Bellville spring made from $60Si_2MnA$, (F) bushing, (G) lower nut, (H) collar shown in Fig. 6, (I) gas chamber, (J) zirconia sliding disk for positioning the upper anvil, (K) steel ball joint for orienting the lower anvil, (L) two WC heaters, (M) metal gasket with hole in center, located between the two anvils, (N) upper and lower observing glass windows, (O) electric connectors for power or thermocouples, and (P1, P2, and P3) gas ports numbered as P1, P2, and P3, as shown in Fig. 2. A–D and F–H are made from SS 304 stainless steel and (K) is made of SS 316 stainless steel.

The HDAC-VII is small enough for use on many equipment stages, including microscope stages and most mounts for x-ray analysis, facilitating its use with many new analytical techniques. The short distance from the sample chamber to the observing window permits the use of small-diameter objective lenses with working distances as short as 13 mm and larger objective lenses, with diameters up to 30 mm and working distances of 17 mm. These dimensions provide adequate separation between the hot sample and lens especially when a small fan is used. Eliminating the long screws in HDAC-VT further prevents serious interference from x-ray emissions and scatter caused by the stainless steel parts between which the x rays had to pass. The large rectangular solid angles are 110° on

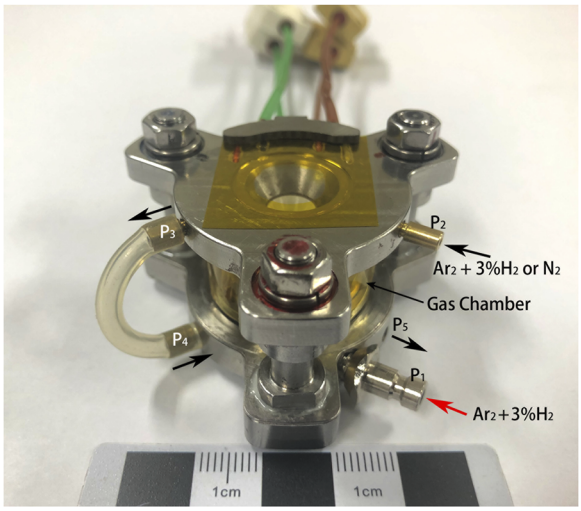

FIG. 2. A photograph of an HDAC-VII; the small scale on the ruler is in millimeters. The Kapton windows can tolerate high temperatures and they enclose the gas chamber to be used for low-energy x-ray analyses. In the heating experiments, the lower large gas port (P_1) is used to deliver gas (Ar or He + 3% H_2) into the gas chamber to prevent the heated parts from being oxidized. At the same time, four connected small gas ports (P_2 to P_5) deliver the mixed gas into the upper and lower spaces between the table faces of diamond anvils and glass windows in order to prevent the table faces of diamond anvils from being oxidized and to cool the observing windows. In the freezing experiments, the four small gas ports will deliver room-temperature N_2 to prevent frosting on the observing window.

three sides when side access is used (Fig. 1), and the sample chamber of HDAC-VII is closer to the side-opening space than that of HDAC-VT, thus allowing easy access for sample loading even when the upper anvil is held just above the lower anvil for rapid closing of the sample chamber. It also provides easier viewing of the sample from the side and allows most x-ray sources and detectors to be placed closer to the sample when cross-axis geometry is used for

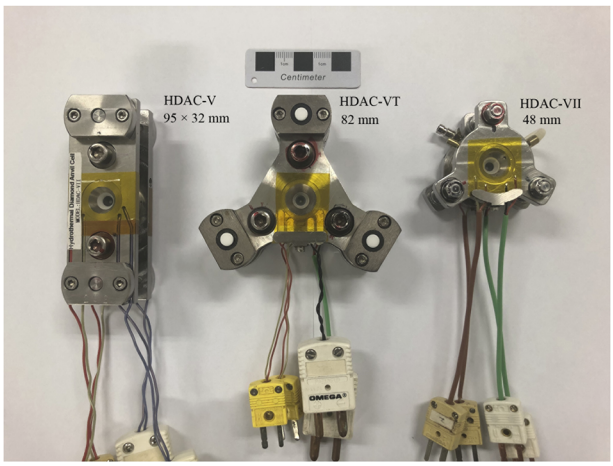

FIG. 3. Photographs of HDAC-V, HDAC-VT, and HDAC-VII showing their different structures and dimensions; the small scale on the ruler is in mm. The horizontal size of each HDAC is noted.

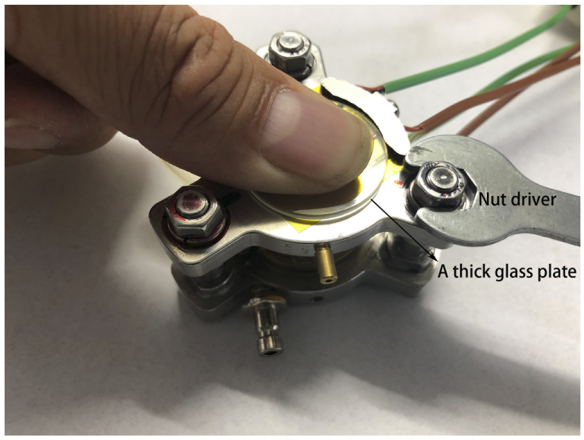

FIG. 4. Photograph showing the closing of HDAC-VII by one person. In this operation, one thumb presses the upper platen while one thick glass plate covers and hence protects the glass window shown in Fig. 2 and the other hand turns the nuts on the threaded posts to seal the sample chamber.

x-ray studies. Additionally, the small size of HDAC-VII makes it easier to assemble HDAC when loading a sample into the chamber by one person, as shown in Fig. 4. That is, we can use one thumb to press the upper platen and another hand to turn the screws when sealing the sample chamber.

The small dimensions also decrease the heat-losing areas in the HDAC body; the body surface is as hot as 60 °C without cooling by using a small fan, when the sample chamber is heated up to 900 °C. In addition, the mixture gas of H_2 and Ar, used to protect diamond anvils and other hot parts from being oxidized, is still hot while venting from the gas chamber. If a small hole drilled in the glass observing window is employed as a vent, as in earlier designs, the hot gas could damage lenses and various types of detectors above the observing window. Therefore, we drilled four ports on the two sides of the upper and lower platens of HDAC-VII for the mixture gas to vent through (Figs. 1 and 2). The four ports can be used to connect the upper and lower cells between the table faces of diamond anvils and glass windows. The mixture gas of H_2 and Ar can enter into the two cells from one upper gas port and vent from one lower gas port, in order to prevent the two table faces of diamond anvils from being oxidized during heating. As a result, this improvement prevents the hot mixture of gases from venting toward the lens and effectively cools the observing windows during heating, ensuring that the lens can be used to observe the HDAC sample chamber for a long time. Moreover, it gets rid of the difficult operation to drill holes in the glass windows and channels in ceramic heat barrier in the upper platen and hemispheric rocker in lower platen for venting of mixture gas from gas chamber shown in Figs. 1 and 2.

III. COOLING SYSTEM OF HDAC

In the cooling system, we used cold nitrogen gas to cool the sample chamber to as low as −170 °C. As shown in Fig. 5, in the cooling system, the nitrogen gas from the gas cylinder first enters into a small liquid nitrogen Dewar flask through a tube coil to be chilled. The tube coil consists of stainless-steel tube with an inner

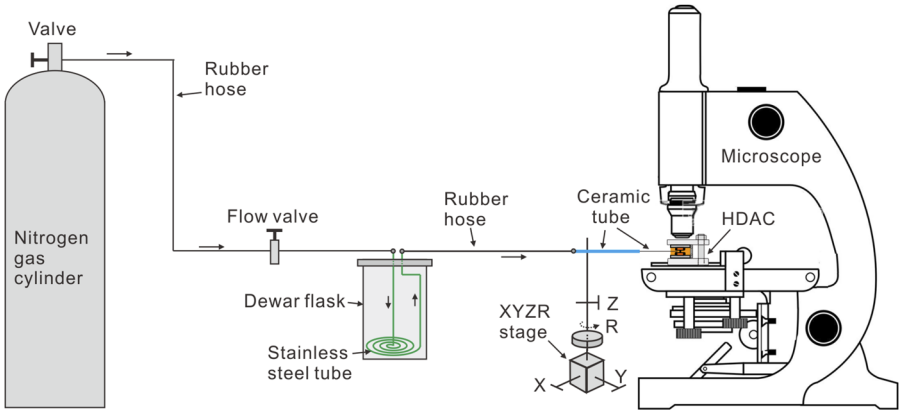

FIG. 5. The schematic diagram of the freezing system for HDAC.

diameter of 1/16 in. and an outer diameter of 1/8 in. The tube coil is located in the bottom of the liquid nitrogen Dewar such that the nitrogen gas can be cooled until the liquid nitrogen in the Dewar is used up. Subsequently, the nitrogen gas cooled in the Dewar blows on the sample chamber through a ceramic tube with an inner diameter of about 1.0–1.5 mm. The ceramic tube is fixed on a XYZR stage that can move the ceramic tube in horizontal and vertical directions and rotate it about the vertical axis through a range of angles, ensuring that the upper and lower diamond anvils will be cooled synchronously with the same temperatures and cooling rates. It is essential to ensure the sample chamber has a uniform temperature such that it can be obtained by averaging the temperatures of the upper and lower diamond anvils. In order to obtain high cooling efficiency for the sample, we attached metal foil to the half-seal collar used for the gas chamber in high temperature experiments to minimize heat transfer (Fig. 6). To prevent condensation on the table faces of anvils and glass observing windows, room-temperature dry nitrogen gas is introduced into the upper observing window chamber and out from the lower observing window chamber through four connected gas ports in the HDAC-VII (Figs. 1 and 2).

In the freezing experiments, the HDAC sample chamber can be cooled to −170 °C. The cooling rate and the subsequent reheating rate of the frozen sample can be controlled by adjusting the flow rate of nitrogen through two valves. The first valve in the exit of nitrogen gas cylinder can be used to coarsely control the flow rate of nitrogen, and the second valve between the nitrogen gas cylinder and the small liquid nitrogen Dewar can be used to fine control the flow rate (Fig. 5). Also, the cooling and reheating rates can be controlled by moving the ceramic tube near to and far from the sample chamber through the movement of the XYZR stage. As shown in Fig. 7, the heating rate of a frozen sample can be controlled to be as low as ~0.1 °C/min, and the temperature differences between the upper and lower diamond anvils could be controlled to be 0.1 °C under the heating rate of less than 1 °C/min. Besides, the reheating process of a frozen sample can be further controlled in high precision by using the HDAC temperature controller (PES1300, see "http://www.pesenterprise.com/products/hdac-cell/"),

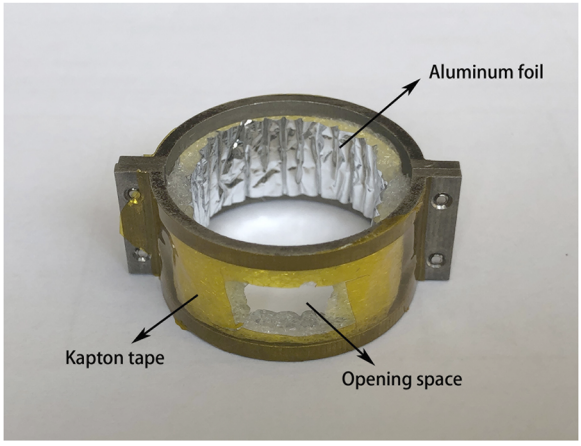

FIG. 6. Photograph of collar used in the freezing experiments, which will replace the collar used in the heating experiments. It is attached with Kapton tape in the outer faces and with aluminum foil in inner faces. The side opening space in the collar is designed for the ceramic tube to deliver cool nitrogen gas to blow on the HDAC sample chamber.

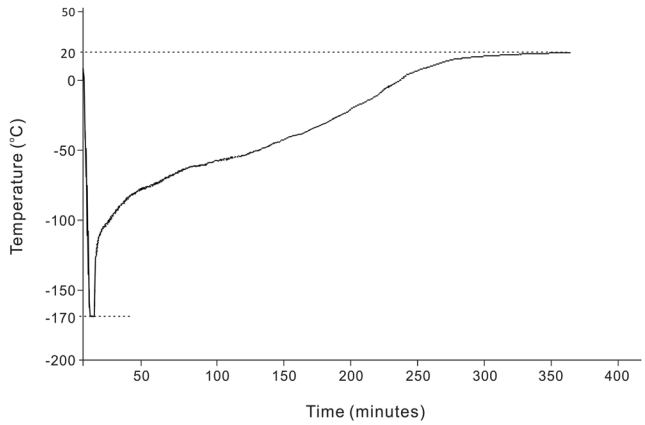

FIG. 7. Temperature curve of the sample chamber in an HDAC-freezing experiment by using the cool nitrogen gas alone. In this experiment, the HDAC-VII sample chamber was first cooled to −170 °C, and subsequently, the temperature increased slowly as shown by the curve.

which automatically controls the power on the heaters of HDAC according to the set heating rate, while cooling with cold nitrogen gas. As shown in Fig. 8, the reheating process can be programmed with PES1300 to heat at certain rates and hold at a certain temperature, and the temperature differences between upper and lower diamond anvils can be no more than 0.1 °C under low heating rates. When the heating temperature, controlled only by the flow rate and/or direction of the cold nitrogen gas, is closer to the actual temperature measured with PES1300, the heating curve of temperature–time was straighter with the temperature fluctuations of 0.1 °C and occasionally 0.3 °C under low heating rates [Fig. 8(a)], and the temperatures of upper and lower diamond anvils were closer [Fig. 8(b)]. Therefore, it is necessary to adjust the flow rate of the cold nitrogen gas to match the heating process set with PES1300 in the freezing experiments.

In order to obtain the correct temperatures of the sample chamber in freezing experiments, the K-type thermocouples were attached on the diamond anvils at the side away from the flow of gas from the nitrogen-blowing tube and buried deeply in cement. Otherwise, the thermocouples could measure temperature of cooled nitrogen gas, rather than diamond anvils or sample. The temperatures in freezing experiments were calibrated with pure water and NaCl–H_2O solution. In our freezing experiments of pure water, the ice finally melted at −0.1 °C, which is close to the triple point of H_2O (0.0 °C). The NaCl–H_2O solution was first cooled to −90 °C, and then heated at the rate of 5 °C/min. When the temperature was close to the eutectic point, the heating rate was decreased to 0.5 °C/min, and the initial melting at −21.0 °C was observed (Fig. 9), which is consistent with the eutectic point of NaCl–H_2O (−20.8 °C, Roedder, 1984; −21.2 °C, Mao and Duan, 2008). Therefore, the temperature accuracy is ±0.2 °C between 0.0 °C and −20.0 °C in our cooling system and less than ±0.5 °C between −170 °C and 1000 °C, as reported by Bassett *et al.* (1993).

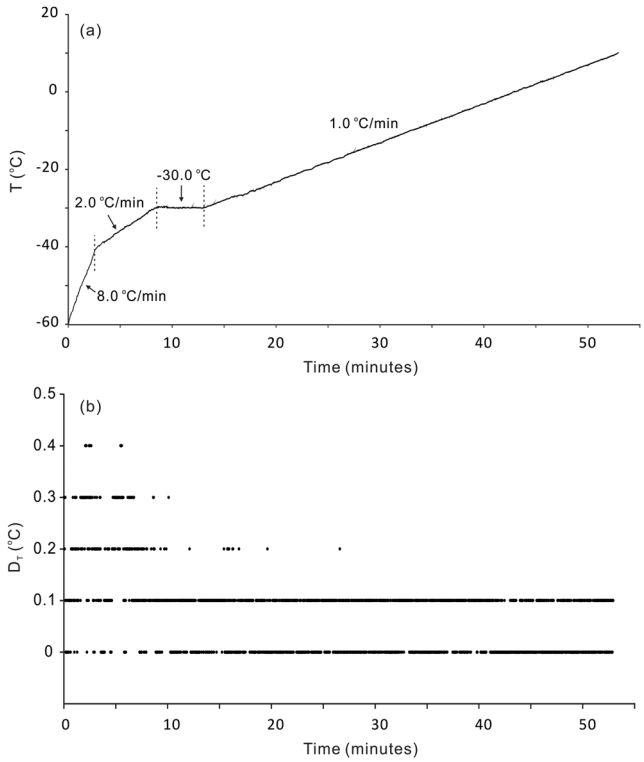

FIG. 8. Temperature curve of the sample chamber that was heated by using temperature controller (PES1300) and cool nitrogen gas concurrently. In this experiment, the temperature controller program was set to warm the sample chamber from −60 °C at rates of 8.0 °C/min and 2.0 °C/min successively; subsequently, the chamber was held at −30 °C for 5 min and finally was warmed to 10 °C at a rate of 1.0 °C/min, as shown in (a). In (b), the temperature differences of the lower and upper diamond anvils (D_T) are shown, most of which are no more than 0.1 °C under the heating rate of 1.0 °C/min (after about 13 min).

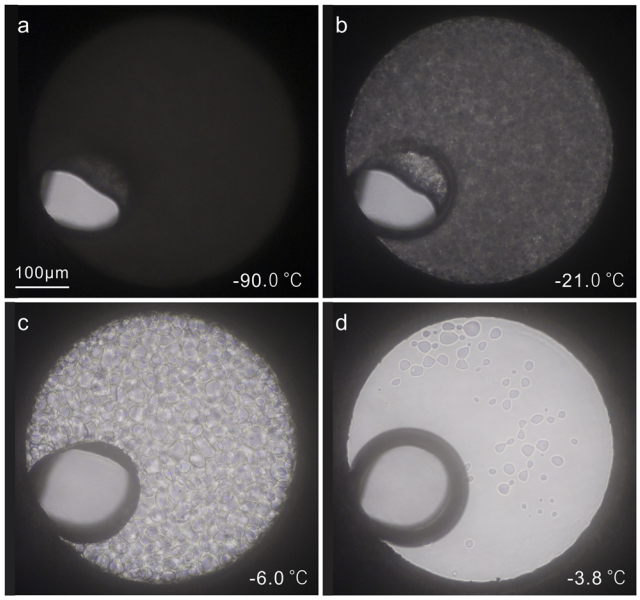

FIG. 9. Photographs showing the H_2O–NaCl-freezing experiments by using HDAC-VII installed with the freezing system. (a) The sample chamber was cooled to −90 °C fast; (b) while temperature increased at a rate of 0.5 °C/min to observe the initial melting at −21.0 °C, which is close to the eutectic temperature of NaCl–H_2O (−20.8 °C, Roedder, 1984; −21.2 °C, Mao and Duan, 2008), indicating the precision in the freezing experiments to be ±0.2 °C, [(c) and (d)] finally, ice totally melted at −3.8 °C, corresponding to the salinity of 6.2 wt. % NaCl based on the EoS of NaCl–H_2O (Mao and Duan, 2008).

IV. APPLICATIONS OF THE HDAC-VII WITH COOLING SYSTEM

The small dimensions make HDAC-VII more easily installed on many sample stages of equipment, including the microscope, x-ray stage, and Raman spectrometer. Moreover, the effective cooling system extends the HDAC applications to low temperatures, especially for the determination of phase relations of fluids.

Here, we introduce three applications of HDAC-VII with the cooling system, including (1) the measurement of NaCl salinity of fluid samples, (2) the determination of H_2O density in the sample chamber with densities greater than 1 g/cm^3, and (3) crystallization of lepidolite in aqueous solution with a salinity of 10 wt. % NaCl.

A. Measuring salinity of NaCl–H_2O solution in HDAC sample chamber

When assembling the upper and lower platens to seal fluid into the HDAC sample chamber, it is inevitable that some fluid will evaporate during assembly. With the application of the freezing system designed as shown in this paper, we compared the true salinities of NaCl–H_2O solution loaded in the HDAC sample chamber with the salinity before loading. In these experiments, the sample chamber consisted of a rhenium gasket with the hole diameter of 0.50 mm and the thickness of 0.125 mm and two anvil faces of 1.0 mm in diameter. The sample solution was first cooled to −90 °C, and subsequently, it was warmed. The warming rate was decreased to 0.5 °C/min to measure the initial melting temperature in order to check whether the temperature is consistent with or close to known eutectic temperature (−20.8 °C, Roedder, 1984; −21.2 °C, Mao and Duan, 2008). During further heating at the same heating rate of 0.5 °C/min, the final melting temperatures of ice (T_m) were measured to calculate the salinity of fluid in the sample chamber based on the equation calibrated for NaCl–H_2O solutions (Bodnar, 1993): wt. % NaCl = 1.78 × Tm − 0.0442 × Tm^2 + 0.000 557 × Tm^3. These experiments showed that NaCl–H_2O solutions with salinities of 1.0 wt. %, 2.0 wt. %, 3.0 wt. %, 5.0 wt. %, 6.5 wt. %, 8.0 wt. %, and 9.5 wt. % NaCl will be concentrated into solutions with salinities of 4.3 wt. %, 6.0 wt. %, 9.0 wt. %, 13.0 wt. %, 15.0 wt. %, 17.0 wt. %, and 20.7 wt. % NaCl, respectively, after loading into the HDAC sample chamber.

B. Determination of water density of more than 1.0 g/cm^3 in freezing experiments

In many hydrothermal experiments using HDAC, pure water was commonly used as a medium to produce pressure within the HDAC sample chamber (Bassett *et al.*, 1993; Schmidt and Ziemann, 2000; Chou, 2003; Schmidt and Chou, 2012; and Li and Li, 2014). Usually, if the inner pressure in the sample chamber was less than 2.0 GPa, water with density below 1.0 g/cm^3 can be used as pressure medium, and water density can be calculated with the vapor bubble-disappearing temperature during heating. However, some experiments were expected to perform under pressure of more than 2 GPa, such as the experiments under plate-subducting condition (Zheng, 2019). As a result, the water must have density of more than 1.0 g/cm^3 to produce expected high pressure in the sample chamber during heating. In such a situation, freezing experiments are essential to measure the ice-melting temperature and subsequently calculate the water density in the sample chamber. In the freezing experiments, different polymorphs of ice can be identified by their distinctive Raman spectra or crystal morphologies, growth patterns, and melting P–T relations such that the final ice-melting temperature can be used to calculate H_2O density at the ice melting T in the sample chamber (Haselton *et al.*, 1995; Chou *et al.*, 1998).

The freezing experiments were shown in Figs. 10 and 11. In the experiments shown in Fig. 10, the pure water was frozen and cooled to −70 °C and subsequently was heated at the rate of 1.0 °C/min. During warming to the ice I + ice III + liquid triple point at −22.0 °C and 209.9 MPa (Wagner *et al.*, 1994), the ice began to melt, showing co-occurrences of ice III and liquid [Fig. 10(c)]. Ice V nucleated and grew fast after warming to ∼−16.8 °C [Fig. 10(d)], being at the ice III + ice V + liquid triple point (350.1 MPa, −17.0 °C, IAPWS, 2011). Finally, ice V melted at −11.9 °C [Fig. 10(f)], indicating that the density of water in the sample chamber was 1.15 g/cm^3 based on the equation of state of water (Wagner *et al.*, 1994). As a result, the pressure at 900 °C was determined to be about 2.9 GPa (Wagner and Pruß, 2002) assuming isochoric relations. In the freezing experiments shown in Fig. 11, the density of H_2O in the sample chamber in the freezing experiments described above was increased by turning the three screws or nuts in HDAC to reduce the volume of the sample chamber. In these experiments, the ice began to melt and

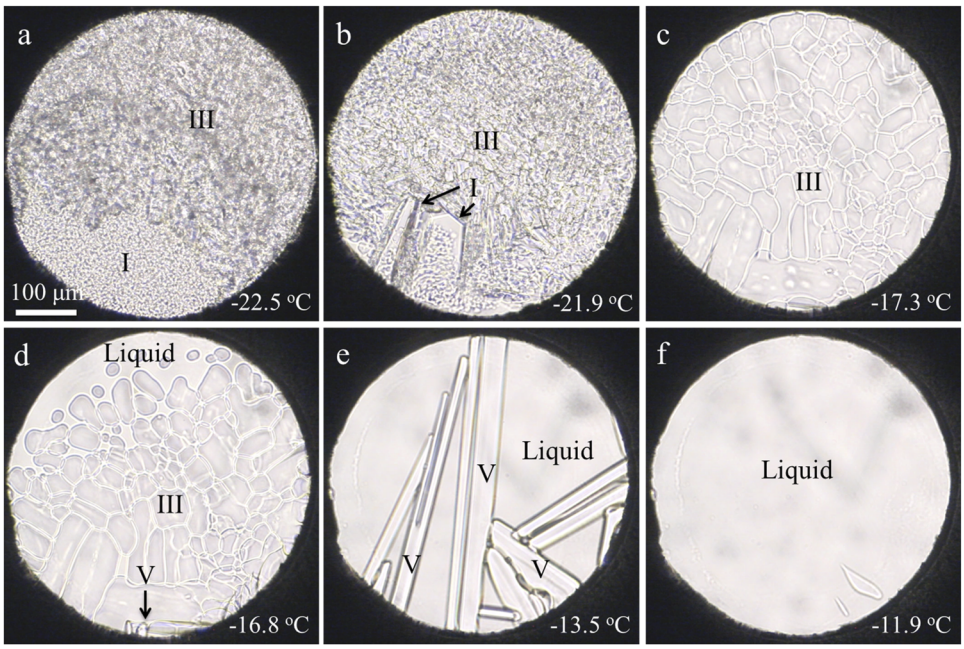

FIG. 10. Photographs showing H_2O ice I-, ice III-, and ice V-melting process in a freezing experiment by using HDAC-VII installed with the freezing system. (a), H_2O ice was warmed to −22.5 °C from −70 °C; (b) during warming up to −21.9 °C, that is close to the ice I + ice III + liquid triple point (209.9 MPa, −22.0 °C, Wagner *et al.*, 1994), ices I and III, and liquid co-existed; (c), at −17.3 °C, ice III melted obviously; (d), ice V nucleated and grew when temperature increased to the ice III + ice V + liquid triple point (350.1 MPa, −17.0 °C, IAPWS, 2011) at −16.8 °C; (e), at −13.5 °C, ice V was growing fast; (f), finally, ice V melted into liquid water at −11.9 °C that was used to calculate the density of water in the sample chamber to be 1.15 g/cm^3 based on the EoS of water (Saul and Wagner, 1989).

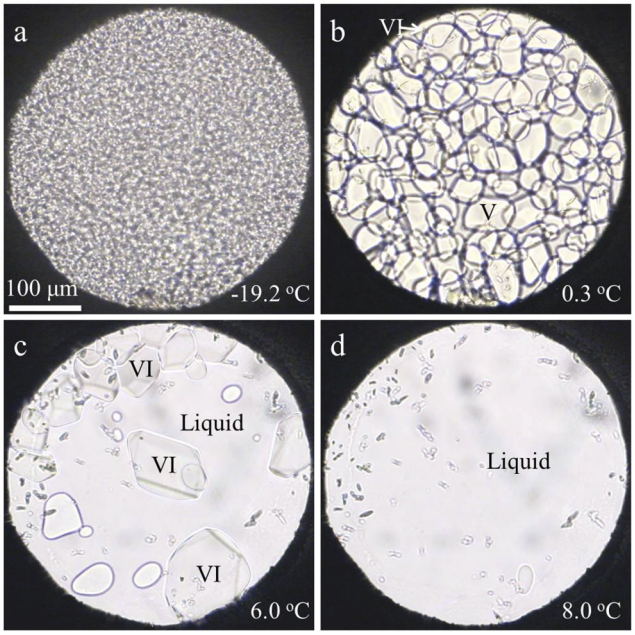

FIG. 11. Photographs showing H_2O ice V- and ice VI-melting process in a freezing experiment by using HDAC-VII installed with the freezing system. (a) During warming from −70 °C, H_2O ice recrystallized at about −19.2 °C near the triple point of ice V + ice III + water (−22.0 °C and 209.9 MPa, Wagner *et al.*, 1994). (b) Nucleation and growth of ice VI at about 0.3 °C near the ice V + ice VI + liquid triple point (632.4 MPa, 0.16 °C, Haselton *et al.*, 1995). (c) Ice VI grew during further warming. (d) Ice VI finally melted into liquid at 8.0 °C, and correspondingly, the density of water in the sample chamber was calculated to be 1.21 g/cm^3 [Wagner and Pruß, 2002; Fig. 2(b) of Haselton *et al.*, 1995].

recrystallize at about −19.2 °C, near the triple point of ice V + ice III + water [Fig. 11(a)], while warming from temperature of −70 °C. Subsequently, ice III began to melt and nucleate ice VI at about 0.3 °C, that is, near ice V + ice VI + liquid triple point (6324 bars, 0.16 °C) [Fig. 11(b); Haselton *et al.*, 1995]. Finally, ice VI melted at 8.0 °C [Fig. 11(d)], indicating that the density of water in the sample chamber was 1.21 g/cm^3 (Wagner *et al.*, 1994) and the pressure will be about 3.6 GPa at 900 °C (Wagner and Pruß, 2002).

C. Crystallization of lepidolite in aqueous solution with salinity of 10 wt. % NaCl

Lepidolite is an important mineral in the rare metal pegmatites and usually crystallized in the late hydrothermal stage during the magmatic-hydrothermal evolution in pegmatite (Heinrich, 1967; Černý, 1989). For example, lepidolite intergrowths with quartz can be found in the core of pegmatite dikes in the Huangnidong pegmatite in Tongcheng, Hubei Province China (Li, 2017). In the Huangnidong pegmatite dike, quartz in the lepidolite-quartz core hosts primary NaCl–H_2O inclusions with a salinity of ~10.0 wt. % $NaCl_{eq}$ and a homogenization temperature of ~300 °C (Li, 2017).

Based on the fluid inclusions in quartz in the Huangnidong pegmatite dike, we crystalized lepidolite in NaCl–H_2O solution with HDAC-VT. In the experiments, natural lepidolite from the Huangnidong pegmatite dike and NaCl–H_2O solution were loaded into the sample chamber of HDAC-VT, producing a Li-, Na-, F-, Cl-rich aqueous solution while lepidolite dissolving into the aqueous solution, similar to the forming conditions of lepidolite-quartz unit in pegmatite (Munoz, 1971 and Gammel and Nabelek, 2016). In this experiment, the salinity of NaCl–H_2O in the sample chamber was determined to be 10.0 wt. % NaCl, calculated based on the final observed melting temperature of ice at −6.6 °C in the freezing experiments, and the vapor bubble-disappearing temperature was adjusted to be 300 °C through tightening the three drive screws to shrink the sample chamber. We heated the sample chamber at the rate of 10 °C/min until the natural lepidolite was totally dissolved into aqueous solution at about 800 °C. Subsequently, the sample chamber was cooled at the rate of 1.0 °C/min, and lepidolite crystallized between 648 °C and 539 °C (Fig. 12). Correspondingly, the pressures of 442 MPa and 301 MPa were calculated with the bulk density of aqueous solution that was determined with the vapor bubble-disappearing temperature based on the EoS of NaCl–H_2O solution from the sample chamber (Mao and Duan, 2008). As a result, we inferred that the lepidolite in the Huangnidong pegmatite dike could form in the P–T conditions between 648 °C, 442 MPa and 539 °C, 301 MPa in a Li-, Na-,

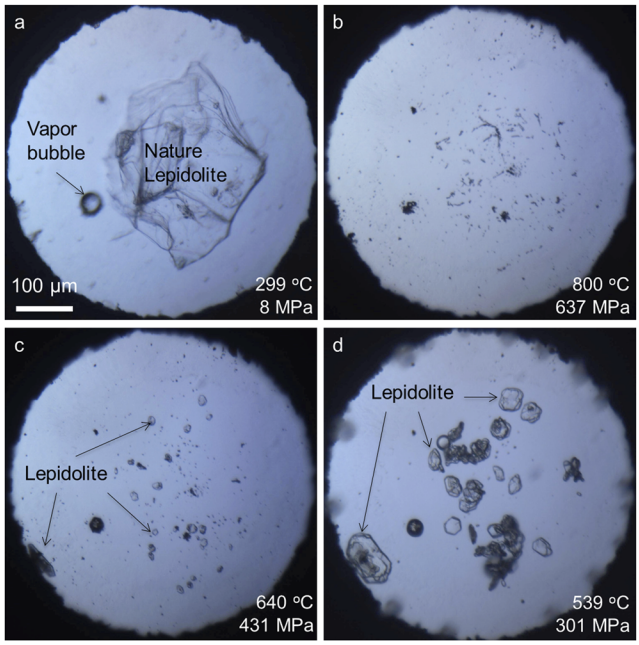

FIG. 12. Photographs showing the recrystallization process of lepidolite in 10 wt. % NaCl–90 wt. % H_2O solution by using HDAC-VII in which the heating process was controlled with PES 1300. (a) In the heating process, the vapor bubble in the HDAC sample chamber almost disappeared at 299 °C and finally disappeared at 300 °C, which was used to calculate the pressure within the sample chamber during heating based on the EoS of NaCl–H_2O (Mao and Duan, 2008). (b) At 800 °C and 637 MPa, the lepidolite totally dissolved into water. (c) At 640 °C and 431 MPa, lepidolite was growing in aqueous solution, which nucleated at 648 °C and 442 MPa in the cooling process. (d) Lepidolite stopped growth at 539 °C and 301 MPa.

F-, and Cl-rich aqueous solution, which is consistent with the pegmatite-forming conditions (London, 2008).

V. CONCLUSIONS

The newly designed HDAC (HDAC-VII) has much smaller dimensions than the previous types, which makes it easy to be installed on a microscope stage for *in situ* observations and micro-analyses. In these applications, it is convenient to have the sample chamber close to the top as well as the side windows such that the objective lens is far enough away from the damaging hot sample and the x-ray source and the detector are close enough to the sample to yield strong signals. At the same time, there is more space for circulating air from a cooling fan. Also, four connected gas ports were designed on the upper and lower platens, which can deliver Ar + H_2 to protect diamond anvils and other parts from oxidation during heating. Dry N_2 gas can pass through the gas ports and direct at the windows to protect them from frosting during cooling.

In this study, a cooling system was designed to accompany the HDAC. In the cooling experiments, nitrogen gas was cooled as it passed through a Dewar flask filled with liquid nitrogen and then blown at the HDAC sample chamber that can be cooled to −170 °C with a precision of ±0.5 °C. The reheating process from a frozen state can be adjusted as low as 0.1 °C/min by using temperature controller (PES) and controlling the flow rate of nitrogen gas with valves concurrently.

The small dimension and the effective cooling system extend the uses of HDAC in geological fluid research. The PTV*x* properties of the fluid loaded in the sample chamber are easily determined in cooling and heating experiments. For example, we determined the salinity of NaCl aqueous solution in the sample chamber and measured pure water density of more than 1.0 g/cm^3 to produce high pressure in the sample chamber at elevated temperature and to perform crystallization experiments in an aqueous solution with known composition.

ACKNOWLEDGMENTS

The authors thank two anonymous reviewers for their constructive reviews. This study was supported by the National Key Research and Development Program of China (Grant Nos. 2019YFC0605203 and 2019YFC0605200), the National Natural Science Foundation of China (Grant No. 41872096), the Chinese National Non-profit Institute Research Grant of CAGS (Grant No. JYYWF201814), and the Key Frontier Science Program of Chinese Academy of Sciences (Grant No. QYZDY-SSW-DQC008).

REFERENCES

Anderson, A. J., Meredith, P., Bassett, W. A., Mayanovic, R. A., and Benmore, C., "The design and application of a new Bassett-type cell for spectroscopic analysis of supercritical aqueous solutions," in *Proceedings of the CNS 2nd Canada-China Joint Workshop on Super Critical Water Cooled Reactors (SCWR), Toronto, Ontario, Canada, 25–28 April 2010* (Canadian Nuclear Society, Toronto, 2010).

Bassett, W. A., "Diamond anvil cell, 50th birthday," High Pressure Res. **29**, 163–186 (2009).

Bassett, W. A., Shen, A. H., Bucknum, M., and Chou, I. M., "A new diamond anvil cell for hydrothermal studies to 2.5 GPa and from −190 to 1200°C," Rev. Sci. Instrum. **64**, 2340–2345 (1993).

Bodnar, R. J., "Revised equation and table for determining the freezing point depression of H_2O-Nacl solutions," Geochim. Cosmochim. Acta **57**, 683–684 (1993).

Bodnar, R. J. and Vityk, M. O., "Interpretation of microthermometric data for H_2O-NaCl fluid inclusions," in *Fluid Inclusion in Minerals, Methods and Applications*, edited by De Vivo B. and Frezzotti M. L. (Virginia Tech, Blackburg, VA, 1994), pp. 117–130.

Černý, P., "Characteristics of pegmatite deposits of tantalum," in *Lanthanides, Tantalun1 and Niobiun Mineralogy, Geochemistry, Characteristics of Primary Ore Deposits, Prospecting, Processing and Applications*, Special Publication No. 7 of the Society for Geology Applied to Mineral Deposits, edited by Möller, P. *et al.* (Springer-Verlag Berlin Heidelberg GmbH, Berlin, 1989), pp. 195–239.

Chou, I-M., "Hydrothermal diamond-anvil cell: Application to studies of geologic fluids," Acta Petrol. Sin. **19**, 213–220 (2003).

Chou, I-M., Blank, J. G., Goncharov, A. F., Mao, H.-K., and Hemley, R. J., "*In situ* observations of a high-pressure phase of H_2O ice," Science **281**, 809–812 (1998).

Gammel, E. M. and Nabelek, P. I., "Fluid inclusion examination of the transition from magmatic to hydrothermal conditions in pegmatites from San Diego County, California," Am. Mineral. **101**, 1906–1915 (2016).

Haselton, H. T., Chou, I.-M., Shen, A. H., and Bassett, W. A., "Techniques for determining pressure in the hydrothermal diamond-anvil cell: Behavior and identification of ice polymorphs (I, III, V, VI)," Am. Mineral. **80**, 1302–1306 (1995).

Heinrich, E. Wm., "Micas of the Brown Derby pegmatites, Gunnison County, Colorado," Am. Mineral. **52**, 1110–1121 (1967).

IAPWS, Revised release on the pressure along the melting and sublimation curves of ordinary water substance, http://www.iapws.org/relguide/MeltSub2011.pdf, 2011.

Li, J., Bassett, W. A., Chou, I.-M., Ding, X., Li, S., and Wang, X., "An improved hydrothermal diamond anvil cell," Rev. Sci. Instrum. **87**, 053108 (2016).

Li, J., Chou, I-M., Yuan, S., and Burruss, R. C., "Observations on the crystallization of spodumene from aqueous solutions in a hydrothermal diamond-anvil cell," Geofluids **13**, 467–474 (2013).

Li, J. and Li, S., "Application of hydrothermal diamond anvil cell to homogenization experiments of silicate melt inclusions," Acta Geol. Sin. (Engl. Ed.) **88**, 854–864 (2014).

Li, P., "Magmatic activities and metallogenic regularity of rare metals of Mufushan area," Post-Doctoral Outbound Report, Institute of Mineral Resources, Chinese Academy of Geological Sciences, in Chinese with English abstract, 2017.

London, D., *Pegmatites*, Canadian mineralogist: Special publication Vol. 10 (The Canadian Mineralogist, Québec, 2008), p. 347.

Maneta, V. and Anderson, A. J., "Monitoring the crystallization of water-saturated granitic melts in real time using the hydrothermal diamond anvil cell," Contrib. Mineral. Petrol. **173**, 83 (2018).

Mao, S. and Duan, Z., "The P, V, T, x properties of binary aqueous chloride solutions up to T = 573 K and 100 MPa," J. Chem. Thermodyn. **40**, 1046–1063 (2008).

Munoz, J. L., "Hydrothermal stability relations of synthetic lepidolite," Am. Mineral. **56**, 2069–2087 (1971).

Roedder, E., *Fluid Inclusions*, Reviews in Mineralogy Vol. 12 (Mineralogical Society of America, 1984), p. 644.

Saul, A. and Wagner, W., "A fundamental equation for water covering the range from the melting line to 1273 K at pressures up to 25000 MPa," J. Phys. Chem. Ref. Data **18**, 1537–1564 (1989).

Schmidt, C. and Chou, I-M., "The hydrothermal diamond anvil cell (HDAC) for Raman spectroscopic studies of geological fluids at high pressures and temperatures," in *Raman Spectroscopy Applied to Earth Sciences and Cultural Heritage*, EMU Notes in Mineralogy Vol. 12, edited by Dubessy, J. *et al.* (Mineralogical Society of Great Britain and Ireland, 2012), pp. 247–276.

Schmidt, C. and Ziemann, M. A., "*In-situ* Raman spectroscopy of quartz: A pressure sensor for hydrothermal diamond-anvil cell experiments at elevated temperatures," Am. Mineral. **85**, 1725–1734 (2000).

Wagner, W. and Pruß, A., "The IAPWS formulation 1995 for the thermodynamic properties of ordinary water substance for general and scientific use," J. Phys. Chem. Ref. Data **31**, 387–535 (2002).

Wagner, W., Saul, A., and Pruss, A., "International equations for the pressure along the melting and along the sublimation curve of ordinary water substance," J. Phys. Chem. Ref. Data **23**, 515–527 (1994).

Zheng, Y.-F., "Subduction zone geochemistry," Geosci. Front. **10**, 1223–1254 (2019).